ELSEVIER

Computers and Geotechnics, Vol. 21, No. 3, pp. 163–182, 1997

Printed in Great Britain
PII: S0266-352X(97)00021-9 0266-352X/97 $17.00+0.00

Effects of End Restraint and Strain Rate in Triaxial Tests

D. Sheng, B. Westerberg, H. Mattsson & K. Axelsson

Department of Civil and Mining Engineering, Luleå University of Technology, S-97187 Luleå, Sweden

(Received 17 January 1997; revised version received 28 April 1997; accepted 13 June 1997)

ABSTRACT

Inhomogeneities caused by end restraint and insufficient drainage during conventional compression triaxial tests are analysed by a numerical method. A finite element model is presented to simulate the testing procedure. The soil–platen interaction is represented by contact elements which allow frictional sliding between contacting nodes. The soil mass is represented by the modified Cam clay model. Coupled hydro-mechanical analyses are carried out in order to simulate both drained and undrained tests. The distributions of stresses and strains in the specimen for different end conditions are compared with the ideal case where no end restraint exists, in order to find representative measuring positions in the sample. Different rates of axial strain are tested in order to study the inhomogeneities caused by insufficient drainage during drained tests. Simulated results show that both end restraint and insufficient drainage can cause the barrel-shape deformation of the specimen. Stress–strain and strength properties based on global measurements are not a good representation of the true material behaviour of one single soil element at constitutive level. © *1997 Elsevier Science Ltd.*

INTRODUCTION

There is no doubt that the triaxial compression test is presently the most widely used procedure for determining strength and stress–strain properties of soils. In such a test, a cylindrical soil specimen is subjected to an axial compression stress σ_a and a radial pressure stress σ_r. The soil specimen is assumed to deform uniformly during the test so that the information obtained from the test represents the true material behaviour of a single soil element. In addition, it is assumed that the axial stress σ_a represents one of

the three principal stresses and the radial stress σ_r represents the other two equal principal stresses. The axial strain, which is assumed to be one of the principal strains, is usually determined based on the measured axial displacement. The radial strain can be either determined according to the radial displacement which is difficult to measure, or more simply calculated from the measured volume change and axial displacement based on the assumption of uniform deformation. It is thus very clear that the uniformity of stress and strain in the specimen is an essential part for the triaxial test concept.

However, it is not often the case that a triaxial specimen deforms uniformly during the test. Non-uniformity can be caused by, e.g. end restraint, insufficient drainage, membrane effects and self weight. The question arises: how much effect does such non-uniformity have on the strength and stress–strain properties determined from a triaxial test? Different researchers have reached different conclusions and a general review of the matter can be found in Lee [1]. Here only a few important conclusions are outlined. According to Lee [1], Taylor concluded in the early 1940s that reliable results could be obtained with soil specimens having regular ends provided their length l to diameter d ratio l/d was in the range 1.5–3.0. Bishop and Green [2] showed, by comparing lubricated and non-lubricated ends, that the end friction had little influence on the measured internal friction angle of sand samples. According to the experimental work by Lee [1], the end restraint could have a significant influence on the undrained shear strength of sand, but just slight effects on the drained strength and on the internal friction angle. The undrained strength of a dense sand tested with lubricated ends was about 20% greater than that with regular ends. Lee attributed this difference to the different changes of pore pressures at failure. Saada and Townsend [3] summarized theoretical elastic solutions of stress distributions at end platens, and found that the vertical stress at the ends of a specimen decreases from a very high concentration at the edge to a lower value at the centre, and that there are no unique patterns for the distributions of radial, circumferential and shear stresses at the ends. Recent work by Shanz and Gussman [4] indicates that the shear strength of an idealised linear-elastic–perfect-plastic triaxial specimen increases with increasing end restraint and is not significantly influenced by sample geometry. Airey [5] studied the effects of different end and drainage conditions in triaxial tests by finite element simulation using the modified Cam clay model. However, the interfaces between the specimen, the rubber layer and the end platens are not effectively simulated, instead continuous displacements are assumed across these interfaces. Isotropically consolidated undrained tests were simulated and the emphasis was put on the consolidation phase. Airey [5] concluded that significant inhomogeneities could occur during isotropic consolidation but their effects on the undrained stress–strain response were small.

The non-uniformity in isotropically normally consolidated clay specimens caused by insufficient drainage in drained tests was studied numerically by Carter [6]. He showed that marked non-uniformity could occur, depending on the relationship between the rate of axial strain, the clay's permeability and the drainage conditions at boundaries. It was also shown that the strength of the clay decreases as the rate of axial strain increases.

In this paper, we will focus our attention on the stress–strain inhomogeneities in a triaxial specimen caused by end restraint in both drained and undrained tests and by insufficient drainage in drained tests. The simulated soil specimen refers to a slightly overconsolidated Swedish clay which, according to Lee [1], should show little effect of end restraint in undrained tests. The problem will be studied by means of numerical simulation using the commercial program ABAQUS [7].

FINITE ELEMENT MODEL

Constitutive model of the soil

To simulate the soil behaviour in a triaxial test, a realistic constitutive model for the soil is needed. Such a model should account for the important features of soil behaviour. During recent years the modified Cam clay model has been considered to be a simple and representative one for cohesive soils. The model is described by an elliptic yield function in the p'–q (mean effective stress–deviator stress) plane, an associated flow rule to define the plastic strain rate, a critical state where unrestricted, purely deviatoric, plastic flow of the soil skeleton occurs under constant effective stresses, and a strain hardening theory that determines the size of the yield surface according to the plastic volumetric strain. Detailed description of the modified Cam clay model can be found elsewhere, e.g. Roscoe and Burland [8] and Muir Wood [9].

Since a soil is a multi-phase medium, deformation of the soil is often accompanied by development of excess pore pressure. The pore pressure change is governed by the continuity equation which is coupled to the equilibrium equation through the rate of pore volume change and the effective stress theory. This is also the theoretical base of soil consolidation. The theory of coupled Biot-type consolidation can be found in Small *et al.* [10].

Soil–platen interaction

The end platens of a triaxial apparatus can be treated as rigid bodies and the soil specimen as a deformable body. In a finite element model, the nodes at the top and bottom surfaces of the specimen are in contact with the rigid

platen surfaces and special contact elements are introduced between the deformable surface and the rigid surface. Between two contacting nodes frictional sliding of a finite amplitude is allowed and any positive pressure can be transmitted. At each integration step these elements construct measures of relative shear sliding. These kinematic measures are then used to introduce surface interaction theories (Sheng *et al.* [11]).

Three different conditions of soil–platen contact are considered:

(1) Perfectly smooth contact (SC), i.e. no friction between the specimen and the end platens.
(2) Frictional contact (FC), with a soil–platen friction angle of 20°.
(3) Completely rough contact (RC), no sliding at contacting surfaces is allowed.

The contact of the first type represents enlarged lubricated end platens, the second type enlarged rough end platens, and the third type rough or smooth end platens which have the same diameter as the specimen and are sealed together with the specimen by a rubber membrane.

Test conditions and material parameters

In order to focus attention on the causes and effects of non-uniformities in triaxial specimens, it was decided to reduce the number of other variables as much as possible. Parameters such as the soil properties, the length to diameter ratio of the specimen, the type of element, the initial stresses, the consolidation pressure and the final value of the global axial strain, are kept constant. In addition, full saturation of the specimen is assumed. The consolidation phase is not considered in this study.

The radial x–y plane of a triaxial specimen, 0.025 m in radius and 0.1 m in height, is discretized into 100 8-node axi-symmetric bi-quadratic elements with pore pressure as the third degree of freedom at corner nodes (Fig. 1). The y-axis is the one of symmetry. The top boundary is in contact with a rigid surface which is only allowed to have vertical movement, while the bottom boundary is in contact with a fixed rigid surface. In a drained test, the top and bottom of the specimen are drained boundaries. The right (circumferential) boundary is subjected to a constant cell pressure of 100 kPa which is equal to the initial stress or isotropic consolidation pressure. The triaxial compression is conducted by controlling the rate and the total value of vertical movement of the top rigid surface. In the case where the effects of end restraint are of interest, a total vertical movement of 0.05 m is carried out during 100 days (8.64×10^6 s). This corresponds to an axial strain of 50% (compressive positive) and a strain rate of 5.79×10^{-8} s^{-1}. Choosing such a large axial strain is motivated by the interest in the soil behaviour at the

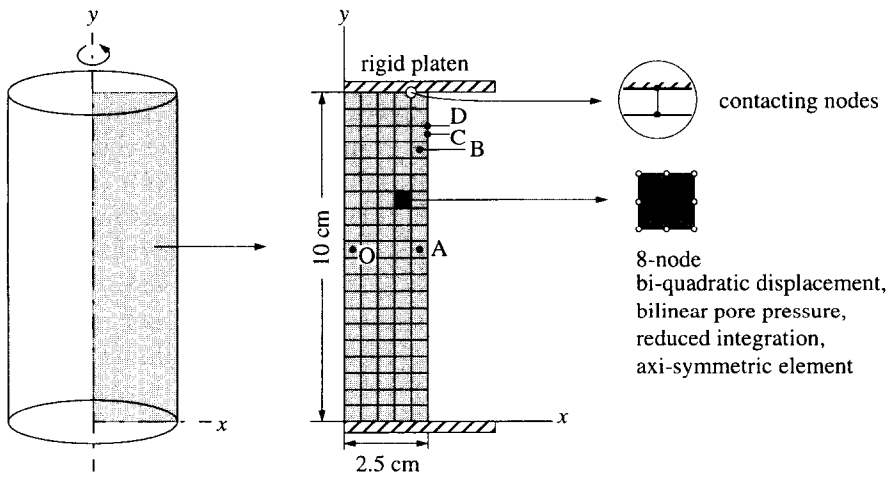

Fig. 1. Finite element representation of the triaxial specimen.

critical state. In the case when the effects of the strain rate are of interest, the same amount of vertical movement is carried out during different time periods, representing different axial strain rates.

The simulated soil is the Norrköping clay (Westerberg [12]) with properties as follows: the initial void ratio $e = 2.5$, the slope of the critical state line $M = 1.2$ in a p'–q diagram (corresponding to an internal friction angle $\phi' = 30°$), the slope of the normal compression line in a $\ln p'$–ε_p diagram $\lambda = 0.2$ (ε_p: volumetric strain), the slope of the unloading and reloading line in a $\ln p'$–ε_p diagram $\kappa = 0.02$, Poisson's ratio $\mu = 0.36$, the initial preconsolidation pressure $p'_0 = 120\,\text{kPa}$ (slightly overconsolidated clay) and the permeability $k = 2 \times 10^{-9}\ \text{m s}^{-1}$.

Global measures of stress and strain

Local stress paths and stress–strain curves will be studied at certain points within the specimen, e.g. the centre point O, the surface point A at the middle height and point B at the 33/40 height (Fig. 1). In addition, global measures of stresses and strains, comparable with laboratory measurements, will be used in this paper. The global axial stress σ_a is either the axial stress applied to the specimen which is the axial force acting on the top platen divided by the current contact area between the platen and the specimen, or the equivalent global axial stress which is the axial force acting on the top platen divided by the current cross-sectional area of the volumetrically equivalent right cylinder. In this paper the former is referred to as the Applied Global Stress Measure (AGSM) and the latter as the Equivalent

Global Stress Measure (EGSM). Both the AGSM and the EGSM are used in practice in triaxial testing apparatuses, but the EGSM is more common. In addition, a theoretical global axial stress defined as the axial force acting on the top platen divided by the current cross-sectional area at point C (Fig. 1) for frictional contact or at point D for rough contact, referred to as the Representative Global Stress Measure (RGSM), will be used for comparison in this paper. The reason for constructing such a global stress measure will be given later. The global radial stress σ_r is equal to the applied cell pressure, as it is usually defined in laboratory testing. The global deviator stress q is the difference between the global axial stress σ_a and the global radial stress σ_r. The global mean stress p is equal to $(\sigma_a + 2\sigma_r)/3$. The global pore pressure u in drained tests is always assumed to be zero, even if the local u is not zero in the cases of insufficient drainage. In undrained tests the local u is uniform within the specimen and the global u takes the value of the local u. The global axial strain ε_a is equal to the vertical movement of the top platen, divided by the initial height of the specimen. The global radial strain ε_r is the average radial displacement divided by the initial radius of the specimen cylinder. The average radial displacement is the difference in radii of the initial cross-sectional area and the current cross-sectional area of the volumetrically equivalent right cylinder.

NUMERICAL RESULTS AND DISCUSSION

Effects of end restraint in drained tests

End restraint or end friction acts as an additional confinement at the ends of a specimen, preventing the soil from moving outwards freely and inducing shear stress. The distribution of the induced shear stress τ_{xy} within the specimen in the drained tests is shown in Fig. 2 for three end conditions at three global axial strains. For the ideal case with perfectly smooth contact, Fig. 2(a),(d) and (g), no shear stress develops in the x–y plane, which means that the axial and radial stresses are indeed the principal stresses. In the cases of frictional and rough contact, shear stresses develop from the end edges into the specimen in an X-shape and increases with increasing axial strain. This X-shape concentration of shear stress can cause localization of shear deformation and eventually result in formation of shear bands (Lade [13]). At large strains significant shear stress τ_{xy} also develops along the lateral surface of the specimen. The soil specimen deforms in pronounced barrel shapes, Fig. 2(h) and (i). More restrained ends lead to a higher shear stress at the end edges and more concentrated displacement in the centre of the specimen, Fig. 2(e) and (h) compared with Fig. 2(f) and (i), respectively.

The occurrence of the shear stress τ_{xy} inevitably causes non-uniform axial and radial stresses within the specimen, which is demonstrated in Figs 3 and 4. The maximum values of effective axial and radial stresses take place at the end edges and the minimum near the 1/2 height of the lateral surface of the

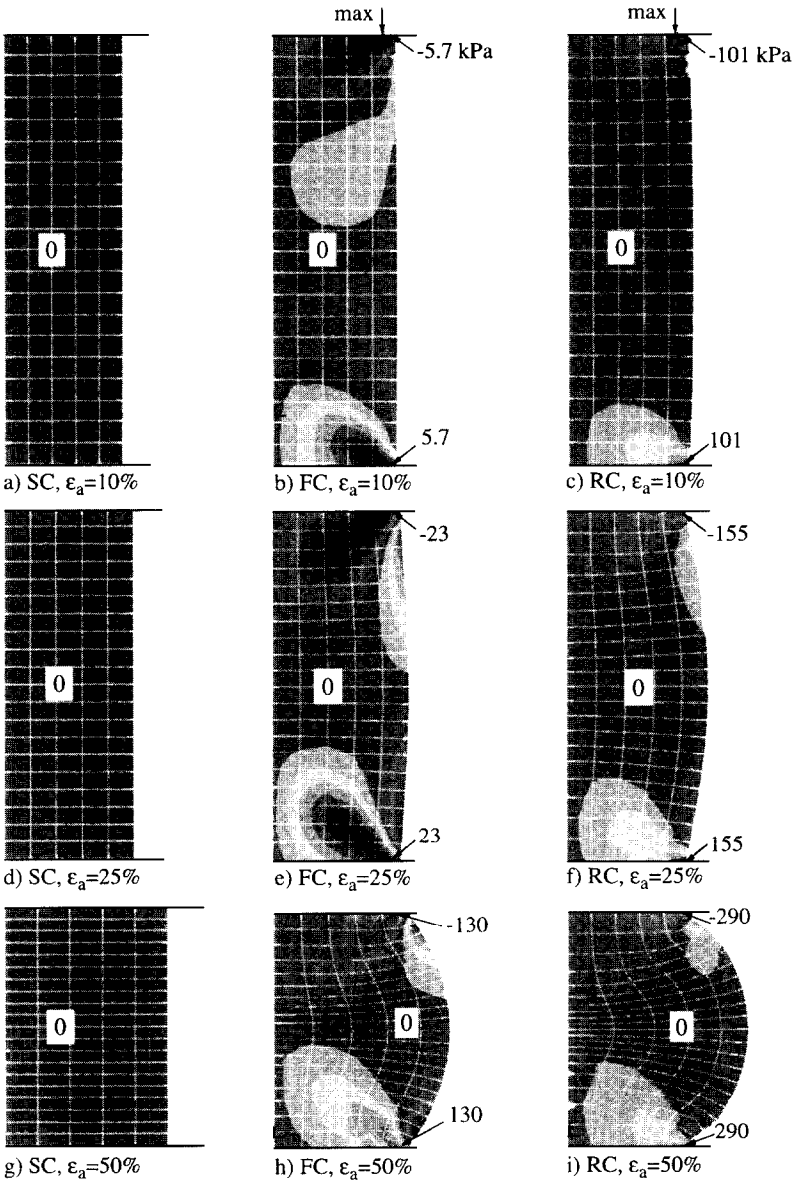

Fig. 2. Distribution of shear stress τ_{xy} (kPa) in specimens for drained tests. (The shear stress is symmetric in the value but differs in sign against the middle plane.)

specimen. The ratio between the maximum and minimum effective axial stress varies from 1.05 for frictional contact at $\varepsilon_a = 10\%$ to 8.0 for rough contact at $\varepsilon_a = 50\%$. The ratio between the maximum and the minimum effective radial stress varies from 1.05 for frictional contact at $\varepsilon_a = 10\%$ to

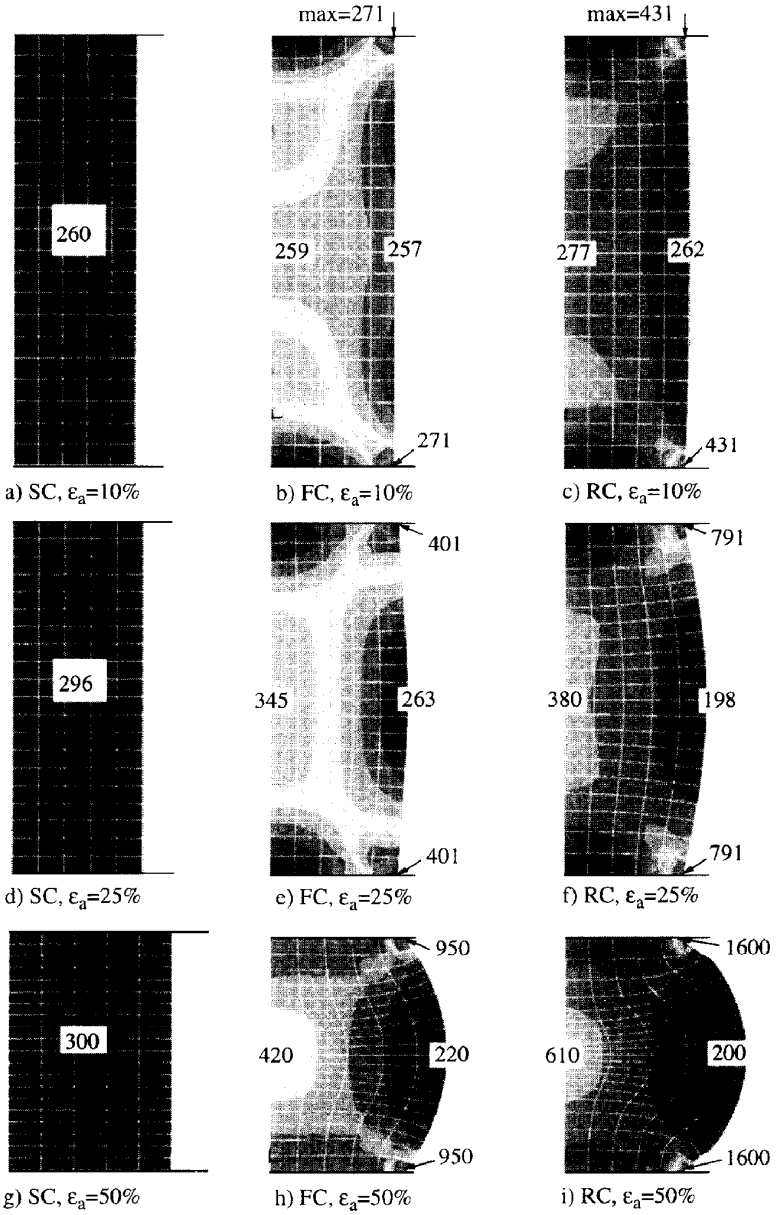

Fig. 3. Distribution of effective axial stress σ'_a (kPa) in specimens for drained tests.

16.7 for rough contact at $\varepsilon_a = 50\%$. In the centre of the specimen, where τ_{xy} is zero and the principal stresses are orientated in the axial and radial directions, the actual effective axial and radial stresses at the end of the tests are, however, higher than those in the ideal case, Figs 3(h) and (i) and 4(h) and (i)

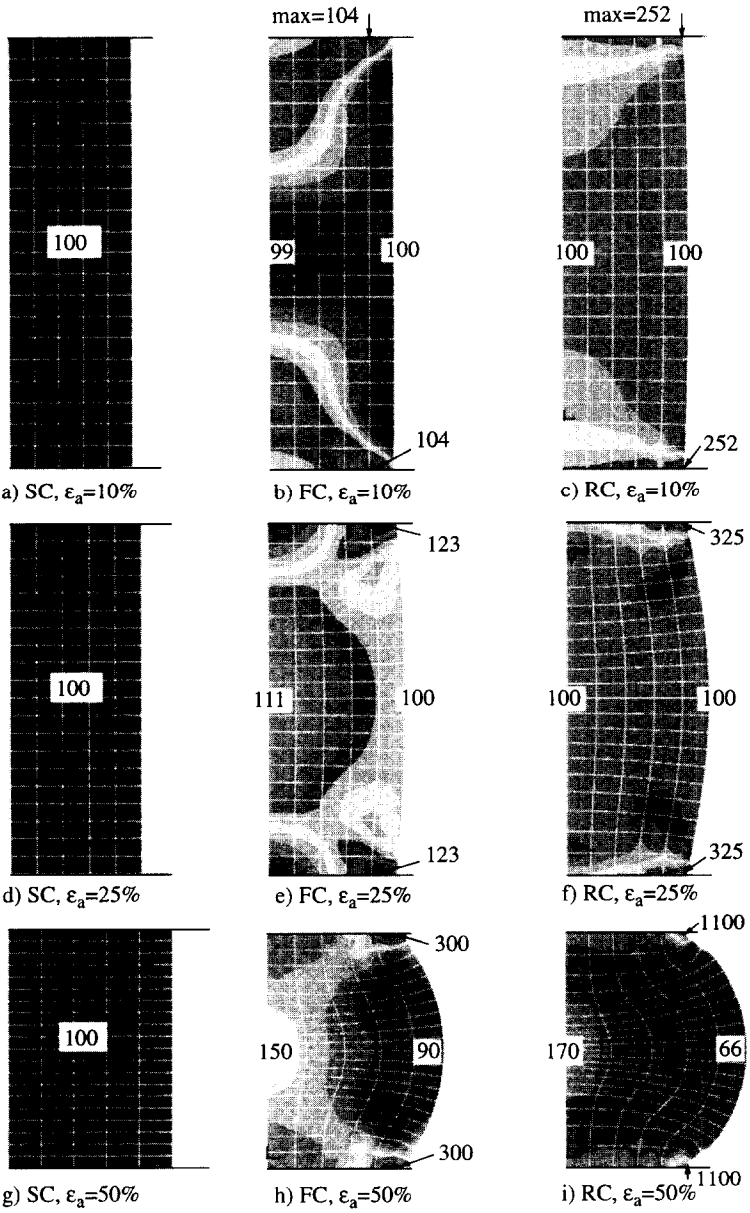

Fig. 4. Distribution of effective radial stress σ_r' (kPa) in specimens for drained tests.

compared with Figs 3(g) and 4(g), respectively. At axial strain levels lower than 10%, the non-uniformities in the stresses are not pronounced, Figs 2(a)–(c), 3(a)–(c), 4(a)–(c).

Compared to the stresses, the axial and radial strains display more pronounced non-uniformities at low strain levels for frictional and rough contact (Figs 5 and 6). It can be noted that the centre of the specimen experiences both the largest axial compression and the largest radial extension, much larger than the global axial and radial strain, respectively. Due to the confinement, the ends of the specimen have the smallest axial compression and

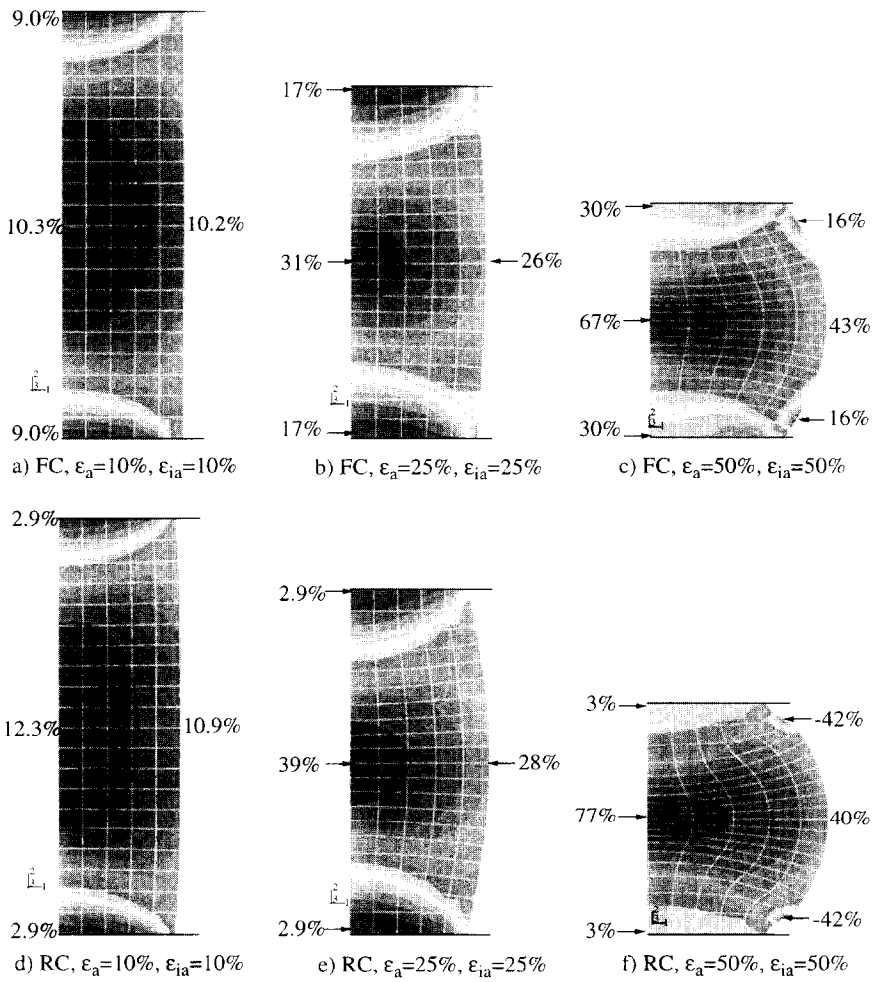

Fig. 5. Local axial strain in specimens for drained tests (ε_a: global axial strain, ε_{ia}: axial strain for the ideal case SC).

the smallest radial extension. Another observation is that the global radial extension, calculated based on the volumetrically equivalent right cylinder for frictional and rough contact at the end of tests, is smaller than the uniform radial extension for the ideal case of smooth contact, Fig. 6(c) and (f). This actually means that the stress non-uniformities due to end restraint have caused larger volume changes or higher degrees of consolidation, which is consistent with the effect of end restraint as an additional confinement.

The stress paths for the drained tests are shown in Fig. 7. The local stress paths at point B (Fig. 1) reach the same critical state position, independent of

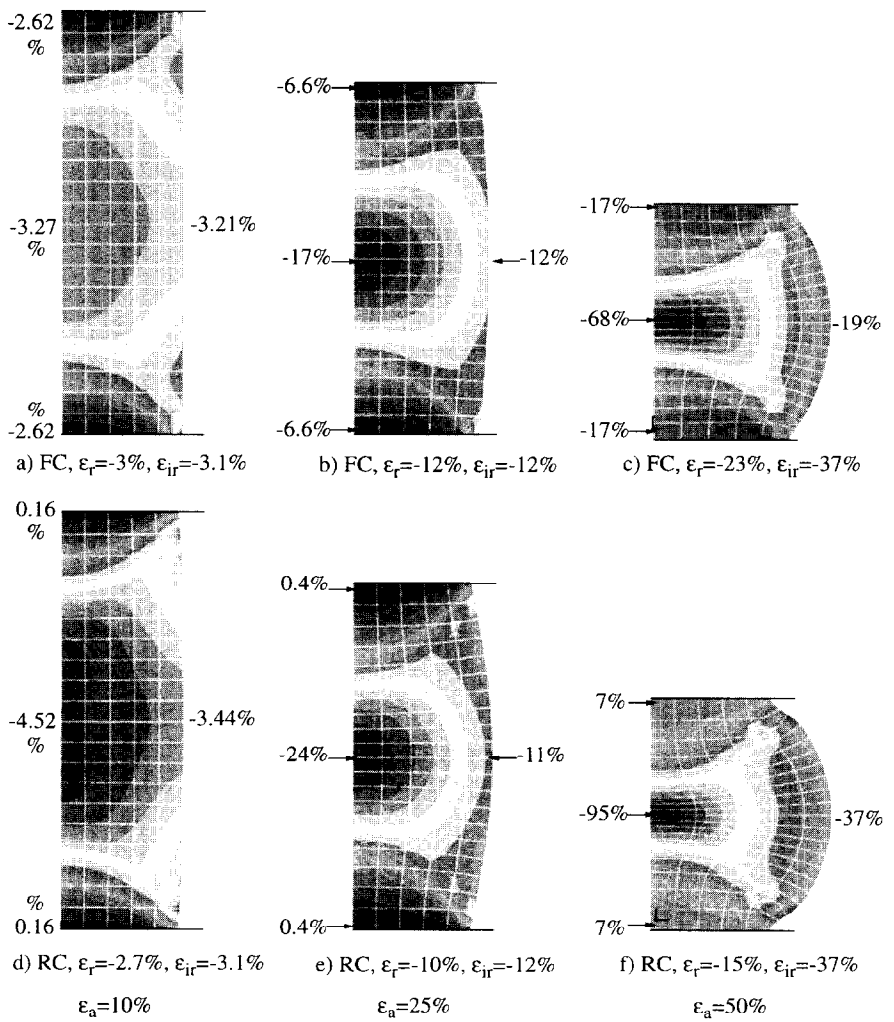

Fig. 6. Local radial strain in specimen for drained tests (ε_r: global radial strain, ε_{ir}: radial strain for the ideal case SC).

end conditions. The stress path at point O first follows the same drained path to the critical state line (CSL) and then moves up, i.e. hardens, along the CSL. This is presumably because this point reaches the CSL earlier than the other points in the specimen, but unrestricted, pure deviatoric plastic deformation at this point is not possible until the surrounding points have reached the CSL.

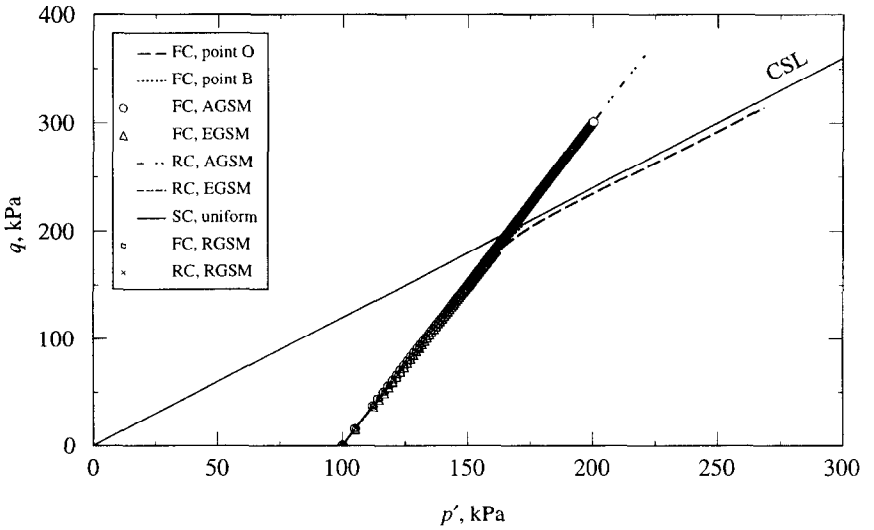

Fig. 7. Stress paths in p'–q plane for drained tests.

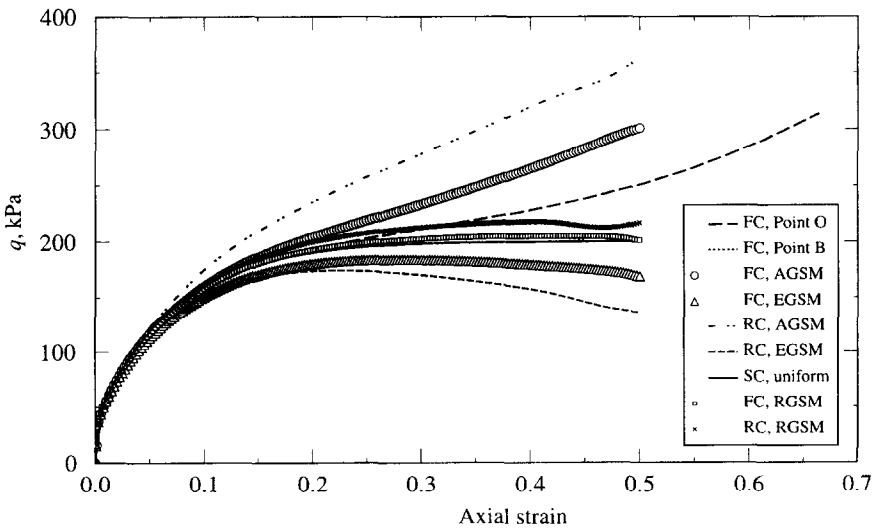

Fig. 8. Deviator stress vs axial strain for drained tests.

In Fig. 7, the global stress paths based on the AGSM and the EGSM with end restraint do not end at the CSL. This is because the global stresses and strains are not only affected by the constitutive law of the material, but also affected by the deformation pattern of the triaxial specimen. In Fig. 8, it can be noted that the drained shear strength is overestimated in the case of AGSM and underestimated in the case of EGSM. The overestimation for the AGSM and the underestimation for EGSM increase with increasing axial strain. Realizing the difference between the definitions of AGSM and the EGSM, i.e. different cross-sectional areas used in calculating the global axial stress, we can presume that an intermediate area, larger than the area of contact but smaller than the area of volumetrically equivalent right cylinder, should result in a better representation of the global axial stress. By testing cross-sectional areas at different heights of the specimen, we find that the global axial stress calculated as the axial force acting on the top platen divided by the current cross-sectional area at point C for the case of FC and at D for the case of RC, gives the best representation of the ideal stress path and the ideal stress–strain curve. This global stress measure is referred to as the RGSM.

Effects of end restraint in undrained tests

In the simulated undrained tests with end restraint, the specimen deforms in similar patterns as in the drained tests but lower maximum shear stresses τ_{xy} are observed (Fig. 9). The non-uniformities in the axial and radial stresses (not shown in the paper) are also similar to those in the drained tests but less pronounced. The pore pressure is uniform in the specimen for all three types of end conditions.

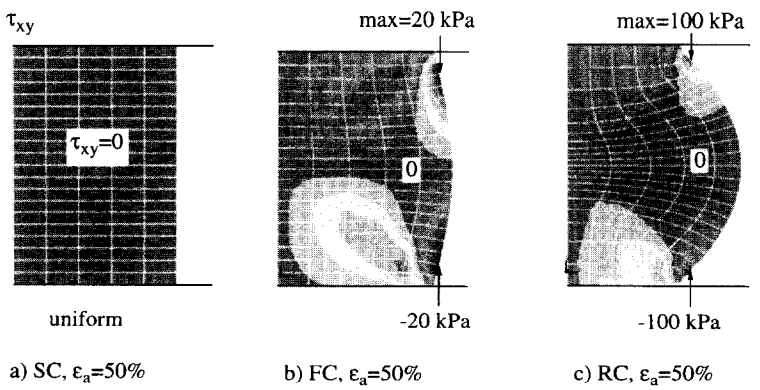

Fig. 9. Distribution of shear stress τ_{xy} in specimens at the end of undrained tests. (The shear stress is symmetric in the value but differs in sign against the middle plane.)

The total volume change in an undrained test is zero. However local volume changes will not be zero if the specimen does not deform uniformly. With end restraint, some parts of the specimen are expected to compress whereas some parts have to swell in order to keep the total volume constant. This is verified in Fig. 10, where contours of local volumetric strains are plotted. In the cases of frictional and rough contact, Fig. 10(b) and (c), volume decreases near the end edges and around the centre (area marked with C), but increases in the outer area of the middle part (area marked with E).

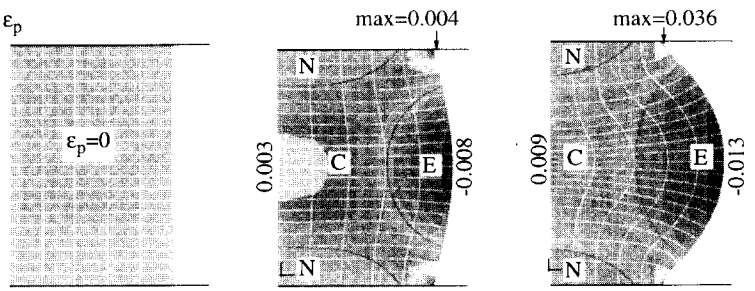

Fig. 10. Local volumetric strain ε_p within specimens for undrained tests (C: volume decrease, E: volume increase, N: no volume change).

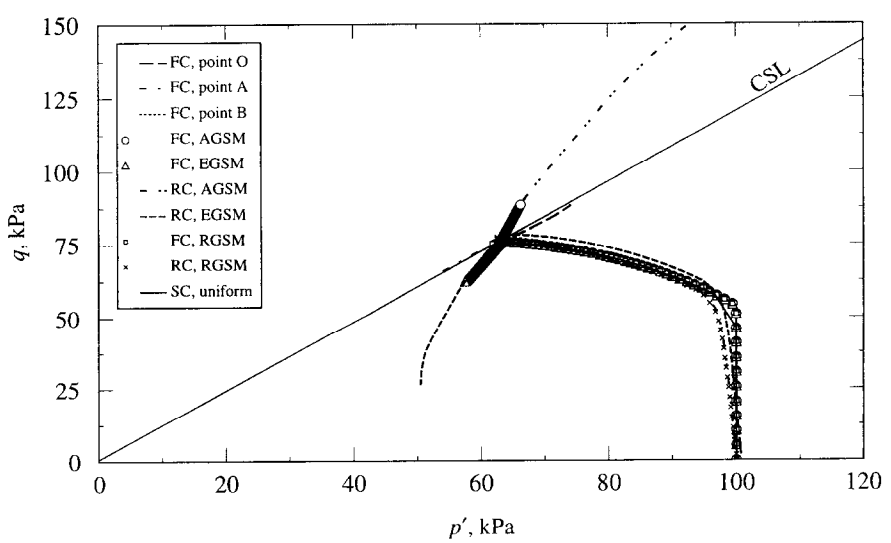

Fig. 11. Stress paths in p'–q plane for undrained tests.

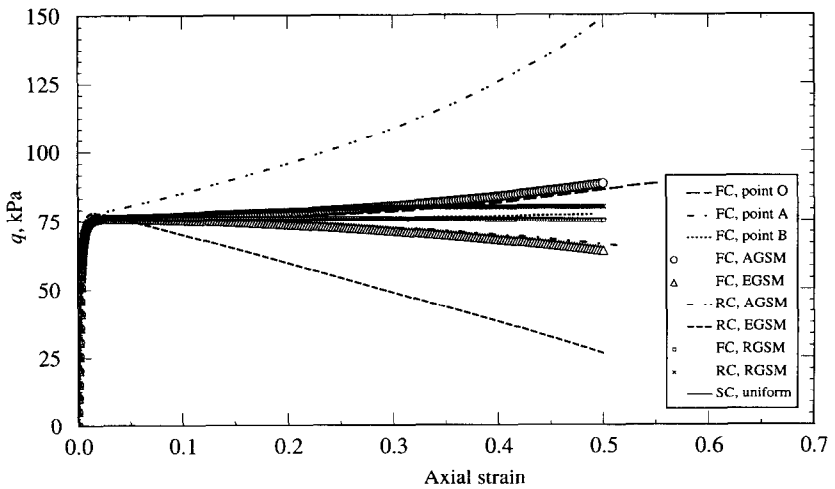

Fig. 12. Deviator stress vs axial strain for undrained tests.

In Fig. 11, the stress paths at point O and point A, after having reached the CSL, undergo, respectively, hardening and softening along the CSL, for the cases of frictional contact and rough contact (not shown in the diagram). This is due to the non-uniform volume changes caused by the boundary conditions. In a saturated soil, a volume decrease means increases in effective stresses such as at point O, and a volume increase means decreases in effective stresses such as at point A. The stress path at point B stays stationary after having reached the CSL because the point lies just on the boundary where no volume change takes place.

The global stress paths based on the AGSM and the EGSM first reach the same point on the CSL and then move respectively over and down from the CSL (Fig. 11), as if the soil were deviatorically hardening and softening, leading to overestimation and underestimation of the undrained shear strength (Fig. 12). Once again we must bear in mind that such a global stress path is not a true material behaviour, but caused by non-uniform deformation of the specimen. Therefore we should be very cautious in interpreting similar experimental observations. The theoretical global stress path and global stress–strain curve based on the RGSM are in relatively good agreement with those for the ideal case, i.e. with smooth contact at the ends.

Effects of strain rate during drained tests

To effectively study the non-uniformities caused by insufficient drainage in drained tests, we eliminate the effects of end restraint here, by assuming perfectly smooth contact between the specimen and the end platens. All

parameters and test conditions are kept the same as described in the subsection *Test conditions and material parameters*, except that the same amount of axial strain is reached within different time periods, corresponding to different strain rates $\dot{\varepsilon}$.

In Fig. 13, it can be observed that the specimen deforms uniformly with $\dot{\varepsilon} = 5.79 \times 10^{-8}(s^{-1})$, whereas in the case $\dot{\varepsilon} = 5.79 \times 10^{-5}\,(s^{-1})$ the specimen deforms in a barrel shape as with end restraint. This barrel-shape deformation

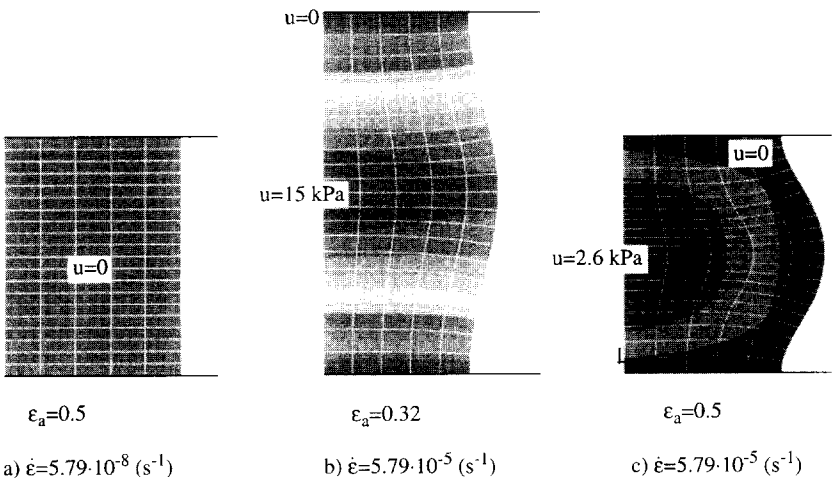

Fig. 13. Effects of strain rate on deformation of the specimen and pore pressure distributions in drained tests.

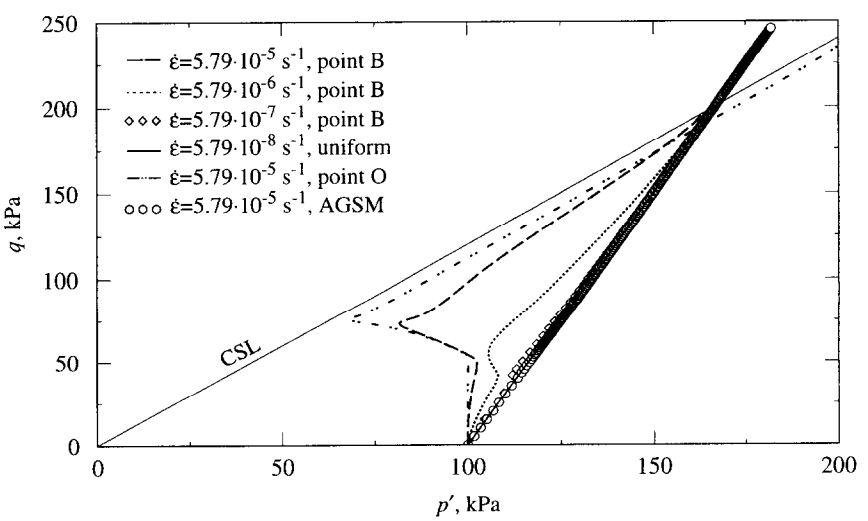

Fig. 14. Effects of strain rate $\dot{\varepsilon}$ on stress paths in drained tests.

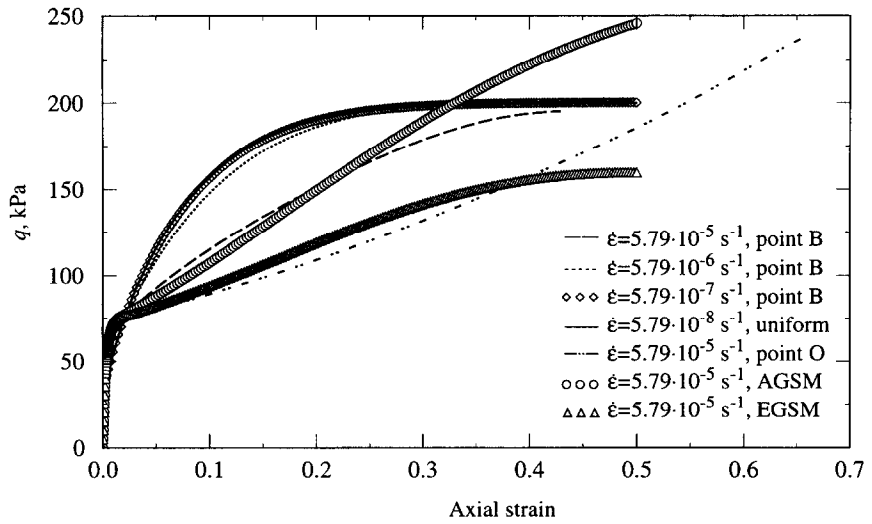

Fig. 15. Effects of strain rate $\dot{\varepsilon}$ on stress–strain curves in drained tests.

under a high strain rate is due to the non-uniform distribution of the pore pressure within the specimen, i.e. drained near the ends but partially drained in the middle part. The soil in the middle part of the specimen is weaker and experiences less volume change. Therefore a larger radial extension is expected to take place in the middle part than near the ends where the soil consolidates. It is also observed that the excess pore pressure in the middle part of the specimen dissipates from outside to inside as the test continues. At the end of the test, the specimen behaves as if drained at all surfaces, Fig. 13(c). The initial undrained behaviour under high strain rates is also shown in the stress path diagram (Fig. 14). The stress path at point B behaves initially undrained, then drained with increasing effective stresses in both axial and radial directions, and finally ends at almost the same critical state position as in the completely drained case. At point O, the stress path first follows the undrained path and approaches the critical state line, thereafter runs along the CSL due to pore pressure dissipation and local yielding as in Fig. 7. The global stress paths or the stress–strain curves under the high strain rates are not in agreement with the actual local stress paths or stress–strain curves within the specimen (Figs 14 and 15).

CONCLUSIONS

In this paper, numerical analyses of non-uniformities in a triaxial specimen caused by end restraint and insufficient drainage have been carried out. It has

been shown that both end restraint in drained and undrained tests and insufficient drainage in drained tests can cause non-uniform barrel-shape deformation of the specimen at large strains. The non-uniformities in stresses and strains increase with increasing strain. The effects of such non-uniformities on stress–strain and strength properties of the soil depend on how and at what strain level these parameters are measured or estimated in triaxial tests. The conventional way of measuring stresses and strains in global terms does not necessarily lead to the true material behaviour of one single soil element. The stress state at the centre of the specimen is also affected by the non-uniformities. According to this study the best representation position for the stress path and the stress–strain curve is located at the 7/40 or 33/40 height at the circumference of the specimen. The use of the global axial stress calculated based on the cross-section area at the 1/8 or 7/8 height for the friction-contact ends and at the 1/10 or 9/10 height for the rough-contact ends also leads to relatively good representation of the true stress path and stress–strain curve.

It has also been observed that the critical state, where pure deviatoric plastic deformation occurs under constant effective stresses, will not be possible for certain positions within a non-uniformly deformed specimen. A stress path along, but not exactly on, the critical state line (CSL) may take place under the following circumstances:

(1) In a drained test with a high strain rate, the soil at the centre of the specimen may first reach its undrained strength and then harden along the CSL due to pore pressure dissipation.
(2) In an undrained test with end restraint, non-uniform local volume changes cause increases and decreases in effective stresses which may lead to hardening and softening along the CSL.
(3) More generally in a non-uniformly deformed specimen, hardening along the CSL may occur at the positions where the stress path has reached the CSL earlier than the other parts of the specimen.

In addition, it has been noticed that a global stress path may, after having reached the CSL, continue moving over or down from the CSL as if the soil were deviatorically hardening or softening. Experimental observations of similar stress paths can be found in the literature. According to this study, such a stress path may be caused by non-uniform deformation of the specimen, but is not a true material behaviour, e.g. deviatoric hardening, of one single soil element at constitutive level. Therefore we should be very cautious in developing new soil models to simulate such an experimental observation, unless we are sure it is a true material behaviour.

Another implication from this study is that boundary effects should be accounted for in calibration of parameters in constitutive models. The

conventional calibration method based on optimization at the constitutive level does not, however, take into consideration those boundary effects. On the other hand, optimization at the finite element level, where the test is viewed as a boundary value problem, should result in a better estimation of model parameters, though this is computationally more expensive (Macari-Pasqualino *et al.* [14]).

Although the results obtained from this study pertain to only one clay and to one constitutive model, the observations are not obviously soil specific and thus should apply to soils of other types.

REFERENCES

1. Lee, K. L., End restraint effects on undrained static triaxial strength of sand. *Journal of Geotechnical Engineering Divisions, ASCE*, 1978, **104**, 687–703.
2. Bishop, A. W. and Green, G. E., The influence of end restraint on the compression strength of a cohesionless soil. *Geotechnique*, 1965, **15**, 243–266.
3. Saada, A. S. and Townsend, F. C., Laboratory strength testing of soils, state of the art. In *Laboratory Shear Strength of Soil, ASTM. Special Technical Publication 740*, ed. R. N. Yong and F. C. Townsend. ASTM, Philadelphia, 1981, pp. 7–77.
4. Schanz, T. and Gussman, P., The influence of geometry and end restraint on the strength in triaxial compression in numerical simulation. In *Numerical Methods in Geotechnical Engineering*, ed. I. M. Smith. Balkema, Rotterdam, 1994, pp. 129–133.
5. Airey, D. W., Finite element analyses of triaxial tests with different end and drainage conditions. *Proceedings of the 7th International Conference on Computer Methods and Advances in Geomechanics*. Vol. 1, ed. G. Beer, J. R. Booker and J. P. Carter. Balkema, Rotterdam, 1991, pp. 225–230.
6. Carter, J. P., Predictions of the non-homogeneous behaviour of clay in the triaxial test. *Geotechnique*, 1982, **32**, 55–58.
7. ABAQUS, *Theory Manual, Version 5.5*. Hibbitt, Karlsson & Sorensen, Inc., Pawtucket, RI, 1995.
8. Roscoe, K. H. and Burland, J. B., On the generalised stress–strain behaviour of 'wet' clay. In *Engineering Plasticity*, ed. J. Heyman and F. A. Leckie. Cambridge University Press, Cambridge, 1968, pp. 535–609.
9. Muir Wood, D., *Soil Behaviour and Critical State Soil Mechanics*. Cambridge University Press, Cambridge, 1990.
10. Small, J. C., Booker, J. R. and Davis, E. H., Elasto-plastic consolidation of soil. *International Journal of Solids and Structures*, 1976, **12**, 431–448.
11. Sheng, D. Axelsson, K. and Magnusson, O., Finite element analysis of cone penetration tests. In *XII Nordic Geotechnical Conference*, ed. S. Erlingsson and H. Sigursteinsson. Icelandic Geotechnical Society, Reykjavík, 1996, pp. 75–85.
12. Westerberg, B., Lerors mekaniska egenskaper (Mechanical properties of clays). Licentiate thesis 1995:02L, Luleå University of Technology, 1995.
13. Lade, P. V., Localization effects in triaxial tests on sand. *Proceedings of the International Union of Theoretical and Applied Mechanics. Symposium on*

Deformation and Failure of Granular Materials, ed. P. A. Vermeer and H. J. Luger. Balkema, Rotterdam, 1982, pp. 461–472.
14. Macari-Pasqualino, E. J., Runesson, K. and Sture, S., Response prediction of granular materials at low effective stresses. *Journal of Geotechnical Engineering, ASCE*, 1994, **120**, 1252–1268.